The mean velocity of the near-field of a lab-scale wind turbine in tailored turbulent shear flows

L. Li, R. J. Hearst, and B. Ganapathisubramani

Abstract This study investigated the mean velocity of the near-field wake of a lab-scale wind turbine subjected to seven different incoming turbulent shear flows through particle image velocimetry. An active grid was used to generate the incoming flows with a novel actuation method that decoupled shear from turbulence intensity. The wake geometry relative to the incoming flows is symmetric and not significantly impacted by shear. A slight reduction in the relative wake velocity deficit was observed at $x/D = 2$ for higher levels of freestream turbulence intensity. The hub velocity contour line was deflected towards the high-velocity side by shear upstream of the rotor. In the wake, higher local shear forced this contour line away from the rotor tip and towards the hub.

1 Introduction

Wind turbine wakes can reduce the power output of subsequent downstream turbines by 20% - 46% (Adaramola and Krogstad, 2011). Velocity fluctuations present in the wakes can also lead to high periodic aerodynamic loads on the blades, shortening lifespans and driving up maintenance costs (Gaumond et al., 2012). It is, however, difficult to create realistic representations of the complex turbulent shear flows found in atmospheric boundary layers (ABLs) in a wind tunnel facility. The shear flow profile is often parameterized for wind turbine applications as a power-law in the form of $U(z)/U_r = (z/z_r)^\alpha$, where z is the vertical direction and $U(z)$ is the freestream velocity profile in the z direction. The subscript r denotes a reference location (Wagner

——————————————

Leon Li

Norwegian Univ. of Science and Technology, Trondheim, Norway, e-mail: leon.li@ntnu.no

R. Jason Hearst

Norwegian Univ. of Science and Technology, Trondheim, Norway, e-mail: jason.hearst@ntnu.no

Bharathram Ganapathisubramani

Univ. of Southampton, Southampton, UK, e-mail: g.bharath@southampton.ac.uk

1

et al., 2011). Dimitrov et al. (2015) showed that α can vary from -0.20 to 0.36, and Wagner et al. (2011) found that 44% of their surveyed shear profiles do not follow this power law. For freestream turbulence, Mücke et al. (2011) found that the turbulence intensity experienced by wind can reach 40%, while typical variations are between 5% to 10%. These studies highlighted the vast parameter space for ABLs, and thus there is merit in determining the impact of shear and turbulence intensity on a wind turbine in general.

Historically, passive flow devices have been used to generate turbulent flows for investigating their effects on wind turbine wakes (e.g. Medici and Alfredsson (2006)). However, these passive methods are limited in the size of the ABL parameter space that they can explore. Active grids offer unparalleled control over inflow conditions since first being popularized by Makita (1991). Recently, several studies have used active grids to generate highly customized inflow conditions for wind turbine or ABL experiments (e.g. Knebel et al. (2011); Neunaber et al. (2017)). Shen and Warhaft (2000) were the first to incorporate an active grid in a turbulent shear flow study by inserting variable solidity screens downstream of the grid. Cekli and van de Water (2010) were the first to create shear flows with an active grid alone. This was accomplished by setting the initial position of the wings to different angles, and then have each set of wings rotate about this angle. Schottler et al. (2017) set their active wings to two different static positions to create a classical and an inverted shear profile. Hearst and Ganapathisubramani (2017) were the first to decouple shear and turbulence intensity. The work by Hearst and Ganapathisubramani (2017) offered unprecedented freedom to explore a large number of parameters for turbulent shear flows with one single setup, and forms the basis for the present study.

2 Experimental Procedure

The open loop suction wind tunnel at the University of Southampton was used for this study. It has a test section measuring 0.9 m × 0.6 m × 4.5 m. The freestream turbulence intensity is approximately 0.2% in the empty tunnel. The active grid used consists of 11 × 7 rods in a bi-planar layout, with mesh length $M = 81$ mm. Control was achieved by 18 daisy-chained stepper motors connected to a computer. The wind turbine model used in this study has a rotor diameter $D = 210$ mm. It is mounted through a sting to the test section floor at a position 3.05 m downstream of the active grid, corresponding to 37.7M. Figure 1 shows the schematic of the setup. The rotor assembly consists of three blades with chord length of 20 mm. The total blockage ratio of the whole model assembly is estimated to be about 2.8%. For all the tests, the turbine was driven at a constant rotational velocity of $\omega = 15$ Hz and the hub velocity U_0 was set to approximately 10 m/s. This gave a tip speed ratio $\lambda \equiv \omega R/U_0 = 1$, where R is the radius of the rotor assembly. The fact that the rotor was motor-driven instead of flow-driven does not impact the wake behaviour under these flow conditions (Araya and Dabiri, 2015). Two pulsed Litron Nd-YAG lasers (532 nm, 200 mJ) were placed side-by-side to illuminate the flow field upstream and

downstream of the wind turbine model. The laser plane coincided with the hub centreline. Two LaVision ImagerProLX 16 mega-pixel cameras equipped with Sigma DG 50 mm lenses were placed along the streamwise direction. The total usable field of view (FoV) was 338 mm × 730 mm. For the laminar uniform flow baseline case, 600 images pairs were acquired, while for all the other test cases 1200 images pairs were taken. All image pairs were acquired at 0.6 Hz. Vector fields were calculated with DaVis 8.4.0 on central processing units through multiple passes from coarse (128 × 128) to fine (32 × 32) grids, with a 50% overlap for each pass. The final spacing between vectors is 1.64 mm. Vector field stitching was done post-calculation in MATLAB.
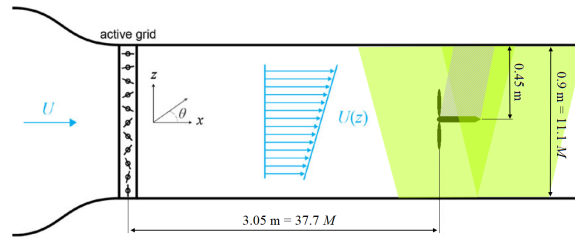

Fig. 1: Schematic of the experimental setup; the grey area is the laser shadow and is represented in later figures as a grey region while the turbine itself is black.

The normalized shear (U_i/U_0) and turbulence intensity (u'/U) profiles are shown in Figures 2a and 2b respectively. Table 1 lists their α and u'/U values. The laminar baseline case is denoted as "LAM", while all the other cases denote shear profiles with a number, and turbulence intensities with L, M, or H for low, medium, or high intensity respectively. For details on the methods used to generate the flow profiles, please refer to Hearst and Ganapathisubramani (2017).
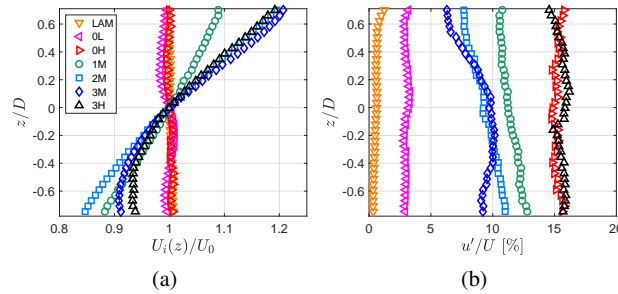

(a)   (b)

Fig. 2: The normalized flow profiles of a) mean streamwise velocity U_i b) turbulence intensity for all cases. The z-axis is normalized by the rotor diameter $D = 0.21$ m.

Table 1: Summary of the flow characteristics at the hub centreline

Mode	α	$u'/U, \%$
LAM	0	0.6
0L	0	3.2
0H	0	14.8
1M	0.17	11.2
2M	0.29	9.2
3M	0.29	9.7
3H	0.24	15.8

3 Mean Velocity Fields

The relative wake velocity deficit (hereafter referred to as the relative wake) is defined as $(U - U_i)/U_0$, where U_i is the incoming flow profile. Its edges are where this field has a value of 0, and its centreline is where the field is minimum. In figure 3a it can be seen that the relative wake edges and centrelines for all cases stay relatively symmetrical about the hub, with no signs of deflections. The different incoming shear profiles and turbulence intensities appear to have no significant impact on the behaviour of the relative wake geometry. The absolute wake velocity deficit (absolute wake) is defined as $(U - U_0)/U_0$, and the hub velocity contour line is traced as the region where $(U - U_0)/U_0 = 0$. In Figure 3b, under uniform flow conditions, these contour lines coincide with the relative wake boundaries and originate from the rotor blade tips. In sheared flows, they are deflected toward the high-velocity side upstream of the rotor. In the near-wake region, shear deflects the hub velocity contour lines from the blade tip toward the hub, and this increases with local shear gradient. This phenomenon can be attributed to the higher momentum carried by the higher shear flows overcoming the radial flows induced by the rotor.

Figure 4a shows the spanwise relative wake profiles at $x/D = 1$, 1.5, & 2 for all cases. Nearly all data points collapse within each wake profile location, which further shows that the macroscopic wake behaviours do not vary significantly with respect to the incoming flow. The two cases with the lowest freestream turbulence intensities have wake profiles that are less smooth, as they lack the promoted mixing found in the cases with higher turbulence intensities (Jin et al., 2016). They also show slightly higher velocity deficits at $x/D = 2$ compared with the others, which is consistent with the findings of Medici and Alfredsson (2006). Figure 4b shows the spanwise absolute wake profiles at the same x/D positions, with the freestream profiles superimposed at $x/D = -0.7$ for comparison with the wake velocity gradients. Shear increases the absolute velocity in the near-wake on the high-velocity side, while the wake core velocity is approximately the same for all cases. They combine to create an absolute wake velocity gradient that is greater than that of the incoming flow, and this effect increases with freestream shear. More investigations are required to examine the wake recovery in the mid and far wake regions to see if subsequent downstream turbines will experience more severe shear flows.
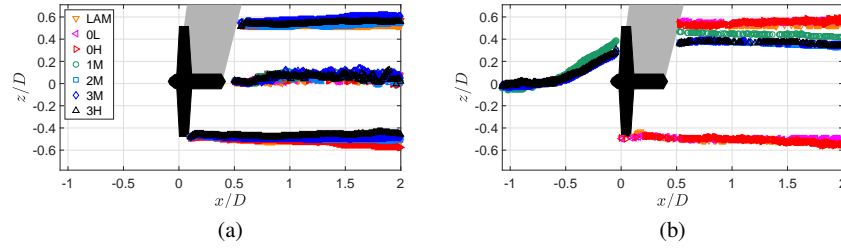
(a)   (b)

Fig. 3: a) The relative wake centrelines and edges of all test cases. b) Hub centreline velocity contour for all test cases.

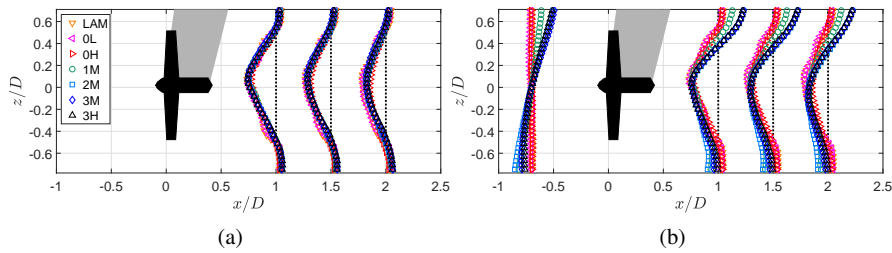(a)   (b)

Fig. 4: The relative and absolute wake profiles at $x/D = 1$, 1.5, & 2 for all cases, where a) is normalized by $(U - U_i)/U_0$ and b) is normalized by $(U - U_0)/U_0$. Wake profiles at $x/D = 1$ is centred at 1, and subsequent profiles are offset by increments of +0.5 from 1. Incoming mean velocity profile is also shown in b) centred at $x/D = -0.7$. The black vertical dotted lines mark $U = U_0$

4 Conclusions

This study used a novel approach to generate seven different turbulent shear flows using a single active grid setup to study the near-wake of a lab-scale wind turbine subjected to these flows. It was found that neither shear nor turbulence intensity has a significant impact on the macroscopic properties of the wake velocity deficit relative to the incoming flow. The absolute wake velocity deficit was skewed by shear flows, with the shear gradient in the wake being greater than that of the incoming flow. The hub velocity contour line was deflected toward the high-velocity side by shear upstream of the rotor. Within the near-wake, increasing shear gradient has the effect of forcing this contour line toward the hub.

Further investigations will look into the turbulence statistics within the same region. As the experimental setup of this study only permitted investigations of wake region up to $x/D = 2$, more studies are required to investigate the mid to far field in the wakes in order to better understand their development and impact on incoming flows faced by downstream turbine installations.

References

Adaramola, M. S. and Krogstad, P. Å. (2011), 'Experimental investigation of wake effects on wind turbine performance', *Renew. Energ.* **36**, 2078–2086.

Araya, D. B. and Dabiri, J. O. (2015), 'A comparison of wake measurements in motor-driven and flow-driven turbine experiments', *Exp. Fluids* **56**.

Cekli, H. E. and van de Water, W. (2010), 'Tailoring turbulence with an active grid', *Exp. Fluids* **49**, 409–416.

Dimitrov, N., Natarajan, A. and Kelly, M. (2015), 'Model of wind shear conditional on turbulence and its impact on wind turbine loads', *Wind Energy* **18**(11), 1917–1931.

Gaumond, M., Réthoré, P.-E., Bechmann, A., Ott, S., Larsen, G. C., Peña, A. and Hansen, K. S. (2012), Benchmarking of wind turbine wake models in large offshore wind farms, *in* 'The Science of Making Torque from Wind 2012: 4th scientific conference'.

Hearst, R. J. and Ganapathisubramani, B. (2017), 'Tailoring incoming shear and turbulence profiles for lab-scale wind turbines', *Wind Energy* **20**(12), 2021–2035.

Jin, Y., Liu, H., Aggarwal, R., Singh, A. and Chamorro, L. P. (2016), 'Effects of Freestream Turbulence in a Model Wind Turbine Wake', *Energies* **9**(830).

Knebel, P., Kittel, A. and Peinke, J. (2011), 'Atmospheric wind field conditions generated by active grids', *Exp. Fluids* **51**, 471–481.

Makita, H. (1991), 'Realization of a large-scale turbulence field in a small wind tunnel', *Fluid Dyn. Res.* **8**, 53–64.

Medici, D. and Alfredsson, P. H. (2006), 'Measurements on a wind turbine wake: 3D effects and bluff body vortex shedding', *Wind Energy* **9**, 219–236.

Mücke, T., Kleinhans, D. and Peinke, J. (2011), 'Atmospheric turbulence and its influence on the alternating loads on wind turbines', *Wind Energy* **14**(2), 301–316.

Neunaber, I., Schottler, J., Peinke, J. and Hölling, M. (2017), Comparison of the development of a wind turbine wake under different inflow conditions, *in* R. Örlü, A. Talamelli, M. Oberlack and J. Peinke, eds, 'Progress in Turbulence VII', Springer International Publishing, pp. 177–182.

Schottler, J., Hölling, A., Peinke, J. and Hölling, M. (2017), 'Brief communication: On the influence of vertical wind shear on the combined power output of two model wind turbines in yaw', *Wind Ener. Sci.* **2**, 439–442.

Shen, X. and Warhaft, Z. (2000), 'The anisotropy of the small scale strucutre in high Reynolds ($R_\lambda \sim 1000$) turbulent shear flow', *Phys. Fluids* **12**.

Wagner, R., Courtney, M., Gottschall, J. and Lindelöw-Marsden, P. (2011), 'Accounting for the speed shear in wind turbine power performance measurement', *Wind Energy* **14**, 993–1004.